PNAS
www.pnas.org

Supplementary Information for

Developmental Topography of Cortical Thickness during Infancy

Fan Wang, Chunfeng Lian, Zhengwang Wu, Han Zhang, Tengfei Li, Yu Meng, Li Wang, Weili Lin, Dinggang Shen, and Gang Li

Corresponding authors: Dinggang Shen and Gang Li.
E-mail: dgshen@med.unc.edu; gang_li@med.unc.edu

This PDF file includes:

SI Materials and Method

Subjects and Image Acquisition. This study was approved by the Institutional Review Board at the University of North Carolina (UNC) at Chapel Hill, School of Medicine. Pregnant mothers were recruited during the second trimester of pregnancy from the UNC hospitals and informed consents were obtained from all the parents. Exclusion criteria include abnormalities on fetal ultrasound and major medical or psychotic illness of the mother. All infants in the study cohort were free of congenital anomalies, metabolic diseases, and focal lesions. All infants were scanned without sedation, and fitted with ear protection, with their heads secured in a vacuum-fixation device. All images in this study were visually checked and rated for motion artifacts using a 4-point visual scale [none (1), mild (2), moderate (3), severe (4)] based on (1, 2). No scan with moderate or severe motion artifact was included in this study. According to the blinded subjective motion artifact rating, the resulted average motion artifact rating for each age group is 1.39 for 1 month, 1.35 for 3 months, 1.38 for 6 months, 1.37 for 9 months, 1.36 for 12 months, 1.39 for 18 months, and 1.35 for 24 months. No strong age-correlation motion has been observed, likely due to the exclusion of scans with moderate or severe motion prior to image analysis. More information about subjects and experiments can be found in (3).

As shown in Fig. S1 and Table S1, totally 210 longitudinal brain MRI scans at around 1, 3, 6, 9, 12, 18, and 24 months of age were acquired from 43 term-born infants (with gestational ages 261~294 days), including 21 males and 22 females. Similar numbers of subjects were acquired at each time point, except that the last time point (24 months) has relatively fewer scans. Of them, 36 subjects have no less than 4 longitudinal scans. Infants were scanned using a Siemens head-only 3T MRI scanner (Allegra, Siemens Medical System, Erlangen, Germany) with a circular polarized head coil. T1-weighted MR images (144 sagittal slices) were obtained by using the three-dimensional magnetization-prepared rapid gradient echo (MPRAGE) sequence: TR (repetition time)/TE (echo time)/TI (inversion time) = 1900/4.38/1100 ms, FA (flip angle) = 7^o, and resolution = $1 \times 1 \times 1$ mm^3. T2-weighted MR images (64 transverse slices) were acquired with turbo spin-echo sequences: TR/TE = 7380/119 ms, FA = 150^o, and resolution = $1.25 \times 1.25 \times 1.95$ mm^3. All images were reviewed by neuroradiologists to ensure sufficient quality.

Image Processing and Cortical Surface Mapping. All T1w and T2w MR images were processed using an infant-specific pipeline detailed in (3), which have been extensively validated in many infant studies (1, 4–10). The preprocessing procedure includes several main steps: 1) Rigid alignment of each T2w image onto its corresponding T1w image and further resampling it to be of $1 \times 1 \times 1$ mm^3 using FLIRT in FSL (11); 2) Skull stripping by a learning-based method (12), followed by manual edit to ensure the clean skull and dura removal; 3) Removal of both cerebellum and brain stem by registration with an atlas (13); 4) Correction of intensity inhomogeneity using the N3 method (14); 5) Longitudinally-consistent segmentation of brain images as white matter (WM), gray matter (GM), and cerebrospinal fluid (CSF) using a dedicated machine learning-based method (15–18); 6) Separation of each brain into left and right hemispheres and filling non-cortical structures.

Inner and outer cortical surfaces of each hemisphere of each MRI scan were then reconstructed and represented by triangular meshes with correct topology and accurate geometry, by using a topology-preserving deformable surface method (19, 20). The inner cortical surface, which has vertex-to-vertex correspondences with the outer cortical surface, was further smoothed, inflated, and mapped onto a sphere (21). Cortical thickness (CT) of each vertex was measured as the minimum distance between the inner surface and the outer surface (19). Longitudinally-consistent inter-subject and intra-subject cortical correspondences were established using a two-stage group-wise spherical surface registration method (3). Accordingly, all cortical surfaces (as well as the attached cortical attributes) were warped into a common space and further resampled to be a standard-mesh tessellation with 163,842 vertices and also smoothed, thus allowing inter-subject and intra-subject vertex-to-vertex comparisons. Considering the computational cost, each cortical surface was further resampled to be 2,562 vertices for discovering the cortical developmental regionalization. Cortical surface reconstruction and registration results have been visually inspected to ensure sufficient quality for subsequent analysis.

Non-negative Matrix Factorization. To reveal the spatiotemporal heterogeneity of CT development of the infant brain, instead of using cortical parcellations predefined according to prior knowledge based on the adult brains, we proposed to discover the infant-specific cortical topography of developmental regionalization of CT by grouping co-developing cortical vertices into the same region. To this end, we adopted the non-negative matrix factorization (NMF) method (22). The main motivation is that NMF can naturally produce a part-based representation of the CT maps of all subjects' scans at all age groups by grouping the cortical vertices changing in a similar manner, thus facilitating the interpretation of the cortical developmental regionalization. Specifically, in NMF, a large non-negative data matrix $\boldsymbol{X}$ is represented by a linear combination of the columns from a non-negative base/component matrix $\boldsymbol{W}$ weighted by the rows from a non-negative coefficient matrix $\boldsymbol{H}$. Mathematically, NMF can be formulated as $min_{W,H \geq 0} ||\boldsymbol{X}\text{-}\boldsymbol{WH}||_F^2$. The non-negative nature of $\boldsymbol{W}$ is attractive due to its high interpretability, and its columns are usually regarded as components, parts, regions, or clusters, depending on different purposes of studies. In our application, $\boldsymbol{X} \in R^{M \times N}$ is a large nonnegative data matrix consisting of CT values from all longitudinal scans of all subjects, where M and N are the numbers of vertices and scans, respectively. By using NMF, $\boldsymbol{X}$ is decomposed into the base/component matrix $\boldsymbol{W} \in R^{M \times K}$ and the coefficient matrix $\boldsymbol{H} \in R^{K \times N}$. The scalar K is the number of components/regions, which is typically small enough, i.e., $K \ll M$ and $K \ll N$.

It is worth noting that, since the large data matrix $\boldsymbol{X}$ in our study included the whole longitudinal course of all subjects, the resulting non-negative elements in each column of the base matrix $\boldsymbol{W}$ naturally point out a group of cortical vertices jointly developing across subjects and ages, thus indicating a distinct region during the developmental regionalization. Specifically, the dimensionality of the data matrix $\boldsymbol{X}$ is 210×4674, which contains totally 210 scans from 43 subjects, and each scan is

represented by the respective CT values at 4674 vertices (after excluding non-cortical vertices). The main motivation of using NMF is that it can naturally identify vertices developing in a similar manner across both subjects and ages, thus uncovering highly interpretable region-based cortical representations. Meanwhile, the NMF method is purely data-driven, without any ad-hoc assumption on the CT changing patterns of vertices. In other words, we included all longitudinal data of all subjects in a large data matrix in NMF to discover groups of vertices that change in similar manners not only across different subjects, but also across different time points (i.e., along development), thereby leading to our desired cortical developmental regionalization.

The solution of $\boldsymbol{W}$ is found following an iterative updating rule (23). Of note, the matrix $\boldsymbol{W}$ signifies a soft vertex-to-region membership, where vertices, especially those on the region boundaries, probably belong to multiple regions. Correspondingly, a hard regionalization can be obtained by assigning each vertex to only one region, which is determined by the maximum weight.

Determination of Region Numbers. To find the appropriate region number K for the NMF method, we jointly considered three widely-adopted criteria, i.e., reconstruction error, instability, and silhouette coefficient.

Reconstruction Error. Intuitively, an appropriate region number should result in a relatively small reconstruction error. Thus, the Frobenious norm of the difference between the original matrix and the data matrix reconstructed by identified components and coefficients was used to quantify the reconstruction error.

Instability. Another view to evaluate the effectiveness of a region number is to consider the stability of the corresponding matrix factorization result (24), as the appropriate region number should be robust to the data. That means, even when only a part of the data is presented, the result should still be relatively consistent with that obtained by using the complete data. To this end, we randomly extracted half of the columns in the data matrix $\boldsymbol{X}$ to form $\boldsymbol{X}_1$, and then extracted the remaining columns in $\boldsymbol{X}$ to form $\boldsymbol{X}_2$. Accordingly, given a region number K, two independent base/component matrices, denoted as $\boldsymbol{W}_1^K$ and $\boldsymbol{W}_2^K$, were generated. The instability between $\boldsymbol{W}_p^K$ (p=1,2) and $\boldsymbol{W}^K$ (derived from the complete data matrix $\boldsymbol{X}$) was sequentially evaluated as in (23) and further averaged. This process was repeated multiple times (10 times in this study) by randomly splitting the data samples at each time.

Silhouette Coefficient. We also adopted the silhouette coefficient to measure the quality of the regionalization results with respect to each specified region number, as this metric is widely adopted for clustering quality evaluation (25, 26). For each vertex v, silhouette coefficient was measured based on its intra-region dissimilarity a(v) and its dissimilarity with other regions b(v), computed as $(min(b(v) - a(v))/max[min(b(v), a(v))])$. A high silhouette coefficient means that the vertex is assigned to an appropriate region. Herein, the dissimilarity between two vertices was computed as one minus their Pearson's correlation between the vectors of their CT values of all scans. The dissimilarity between a vertex and a region was computed as the mean dissimilarity of each vertex with all vertices of that region. The final silhouette coefficient was computed as the average of the silhouette coefficients of all vertices.

Charting Longitudinal Developmental Trajectories. We adopted three parametric models, i.e., the linear, quadratic and sigmoid models, and one non-parametric model, i.e., the generalized additive mixed models (GAMM) (27), to fit the development trajectory of CT in each discovered region. Our motivation to comprehensively test both parametric and non-parametric models is that, CT increases dynamically in the first year and then exhibits region-specific increase or decrease in the second year (4). Therefore, the three parametric models were used to model three different cases, i.e., whether (in the first two years) CT shows 1) a continuous increase (the linear case), 2) an increase first followed by a decrease after attaining a peak (the quadratic case), or 3) an increase first followed by a relative plateau (the sigmoid case). In addition, the non-parametric GAMM was used to handle complex situations more generally in a data-driven way.

Let $y_i(t)$ be the CT for the i-th subject at time t, we fitted $y_i(t)$ in the following four different models: (i) the linear random intercept model $y_i(t) = t+s_i+t*s_i+\alpha_i+e_i(t)$; (ii) the quadratic random intercept model $y_i(t) = t^2+t+t^2*s_i+t*s_i+s_i+\alpha_i+e_i(t)$; (iii) the sigmoid random intercept model: $y_i(t) = 1/(1 + exp(-t - t * s_i)) + s_i + \alpha_i + e_i(t)$; and (iv) the GAMM model $y_i(t) = f(t) + \Delta(t) * s_i + \alpha_i + e_i(t)$. Herein, s_i denotes the sex information (1 for males and 0 for females) of the i-th subject; α_i represents the random intercept effect for the i-th subject; $f(t)$ and $\Delta(t)$ are two nonparametric functions (27) which were fitted with the cubic splines; and $e_i(t)$ denotes the random Gaussian noise for the i-th subject at time t, which are assumed to be independent and identically distributed for $i = 1, 2, \cdots, n$ and $t > 0$. The statistical significances of the fixed effect for all models were assessed through the analysis of variance (ANOVA), and the p-values of the F-statistics are reported in Table S2. To determine the best-fitted model on our data, the general cross validation (GCV) error (28, 29) was estimated following the way in (30), considering that it is commonly used as a metric for the comparison between nonparametric and parametric models (30). The resulting GCV values of all four models are reported in Table S2, based on which GAMM was selected as the best model for all of the regions due to the smallest GCV. After that, the first derivative of the best-fitted model was computed to represent the CT development rate. A peak age was estimated by setting the first derivative of the fitted curve to be zero. If CT in a region shows continuous increase without attaining the peak during the first 2 years, we report that no peak has been found in this region. The detailed peak ages are reported in Table S2. The p-values of the ANOVA F-test to evaluate the significances of the sex difference (summarized in Table S2) were calculated by comparing the full model to the reduced model (i.e., ignoring the sex-related covariates) in the GAMM.

Statistical Analysis.

Peak age confidence interval. We analyzed the confidence intervals of the estimated peak ages (when exist) for all cortical regions. To this end, the longitudinal bootstrap sampling (31) on all subjects was repeated 500 times. Based on the resulting 500 estimations of the peak age for each region, the 0.95 confidence intervals of all peak ages were computed and reported in Table S2.

Significance testing of CT changes between ages. We tested the significance of CT decrease from 18 to 24 months, 14 to 18 months and 14 to 24 months for regions that reach the peak during first two years. Between 18 and 24 months, we selected all subjects with MRI scans at both time points and then used the paired Wilcoxon test to check if the CT changes are significant. For 14 months, which was not included as a scan time point in the data acquisition protocols, we estimated CT values at this age for all subjects based on GAMM. The estimated CT values at 14 months were then compared with CT values at 18 and 24 months using the paired Wilcoxon test. All the resulting p-values are FDR corrected and summarized in Table S3 of the revised paper.

Sample bias testing. It is worth noting that our data had fewer samples at 24 months compared with other time points, which might influence the estimation of CT developmental trajectory. We have investigated this problem in two complementary aspects: First, we have created another data group, by removing those subjects having any missing scan(s) at 12, 18 or 24 months. In this way, only 80 scans from 13 subjects are available (i.e., small-sample data). Similar to the peak ages estimated using all data, this small-sample peak ages were also estimated 500 times through longitudinal bootstrap sampling (31). Unpaired Wilcoxon test was performed to evaluate the differences between the estimated peak ages using all the data and that of using the small-sample data, with results (FDR corrected) reported in Table S4. Second, considering that only a small number of subjects has all scans at both 12, 18 and 24 months, we have also tested that, for each time point, whether infants with follow-up scans at 24 months and infants without follow-up data at 24 months show a distinct group difference of CT. Specifically, we divided all subjects into two groups: 1) those subjects with scans at 24 months and 2) those subjects without scans at 24 months, and applied the unpaired Wilcoxon test to check if there is significant difference between these two groups. The corresponding p-values after FDR correction are reported in Table S5.

SI Results.

Significance testing of CT changes between ages. With the significance level of $p < 0.05$, neither the whole-brain nor any region shows significant decrease of CT from 18 to 24 months, as shown in Table S3. Comparing the CT values at 14 months with CT values at 18 and 24 months, at the whole-brain level, no significant decrease in CT is shown from 14 to 18 months. From 14 to 24 months, the right hemisphere shows significant decrease in CT. At the region level, regions 4, 7, 12, 14, 16 and 17 do not show any peak age during the first two years. Remaining regions have estimated peak age between 350 to 457 days (~11.5 to 15 months). For these regions, from 14 to 18 months, regions 3 and 9 show significant decreases in the left hemisphere, and regions 1, 3 and 9 show significant decreases in the right hemisphere. From 14 to 24 months, regions 1, 3, 6, 9, 10 and 15 show significant decreases in the left hemisphere, and regions 1, 3, 9, 10, 15 show significant decreases in the right hemisphere.

Sample bias testing. With the significance level of $p < 0.05$, according to Table S4, the whole-brain peak age does not show significant difference between using all the data and using only the small-sample data. At the region level, most regions do not show significant differences between these two groups as well. According to the significance reported in Table S5, no significant difference in cortical thickness has been found between infants with follow-up scans at 24 month and infants without follow-up scans at 24 months. This indicates that our estimated peak ages are not biased by the smaller sample size at 24 months.

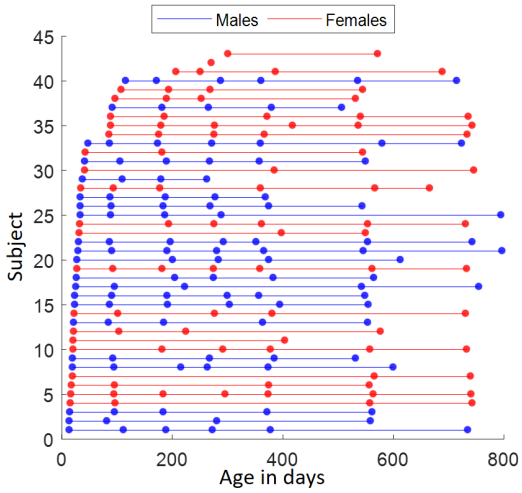

Fig. S1. Distribution of longitudinal scans. Each point represents a scan at its scanned age (in days) shown in the x-axis. Each horizontal line represents one subject, with males in blue and females in red.

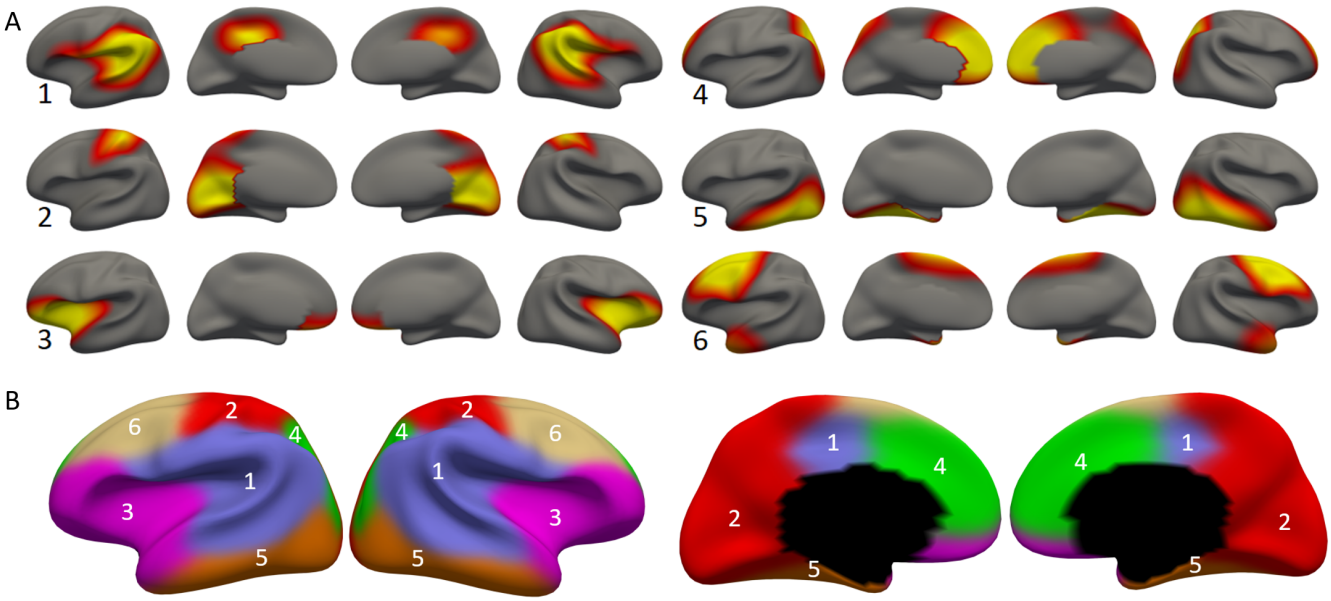

Fig. S2. Developmental cortical regionalization with K=6. (A) Each component is shown in both the lateral view and medial view, with warmer color corresponding to higher values. (B) Hard regionalization map obtained by assigning each vertex to only one region according to the maximum weight. These regions approximately correspond to: 1) perisylvian areas, inferior parietal lobules, and posterior cingulate cortex; 2) medial occipital and dorsal sensorimotor areas; 3) insula and orbitofrontal areas; 4) medial prefrontal and superior parietal lobules; 5) middle, inferior, medial temporal cortices and fusiform; and 6) dorsal frontal cortex and temporal pole.

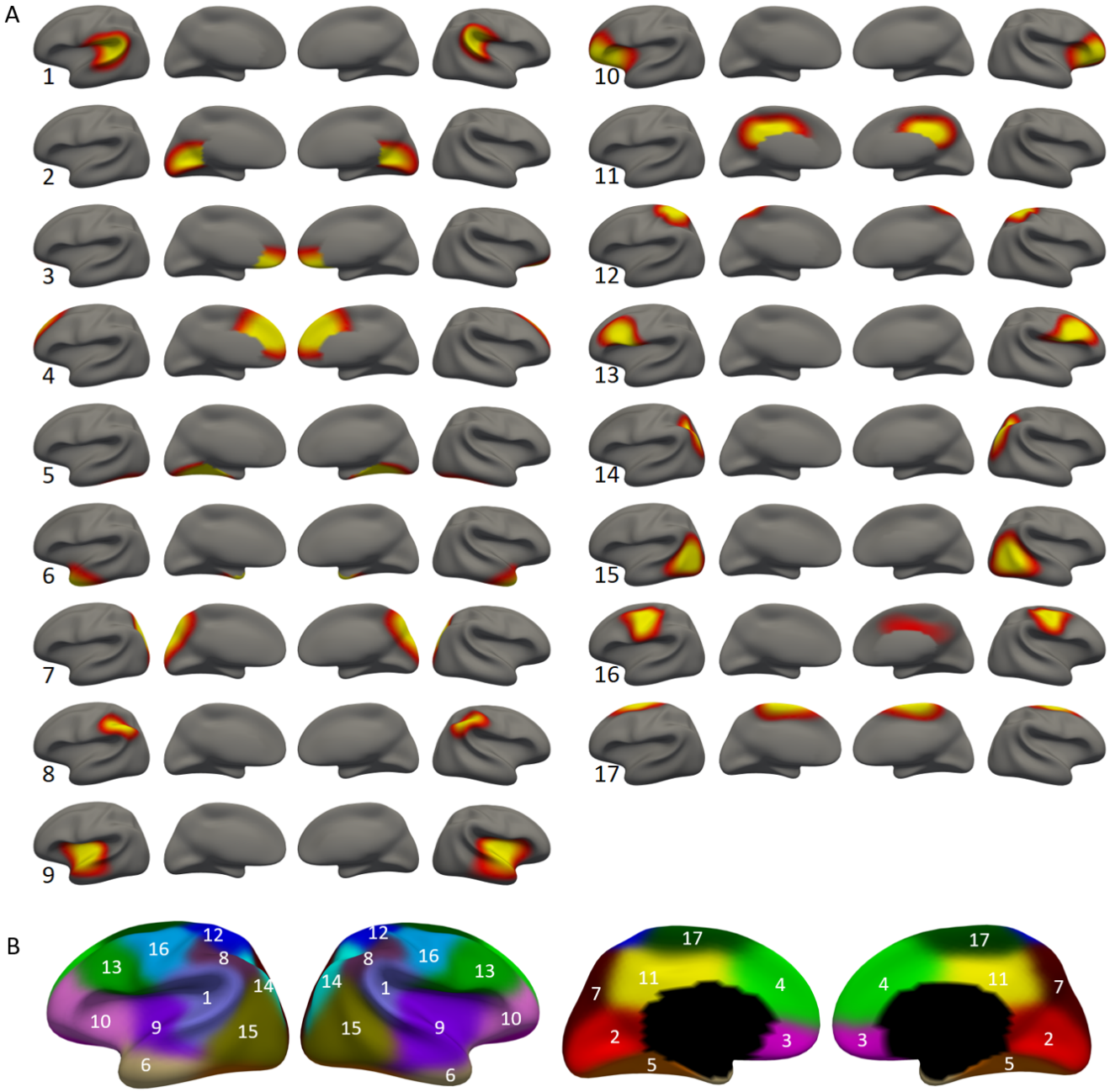

Fig. S3. Developmental cortical regionalization with K=17. (A) Each component is shown in both the lateral view and medial view, with warmer color corresponding to higher values. (B) Hard regionalization map obtained by assigning each vertex to only one region according to the maximum weight. These regions approximately correspond to: 1) perisylvian areas; 2) medial occipital cortex; 3) medial orbitofrontal cortex; 4) medial prefrontal cortex; 5) medial temporal areas and fusiform; 6) temporal pole; 7) precuneus; 8) inferior parietal lobules; 9) middle insula and anterior superior temporal lobe; 10) lateral orbitofrontal and anterior insula; 11) middle and posterior cingulate cortices; 12) dorsal somatosensory area; 13) inferior frontal, triangularis and opercularis; 14) superior parietal lobule; 15) posterior temporal and lateral occipital cortices; 16) sensorimotor areas; and 17) paracentral and superior frontal areas.

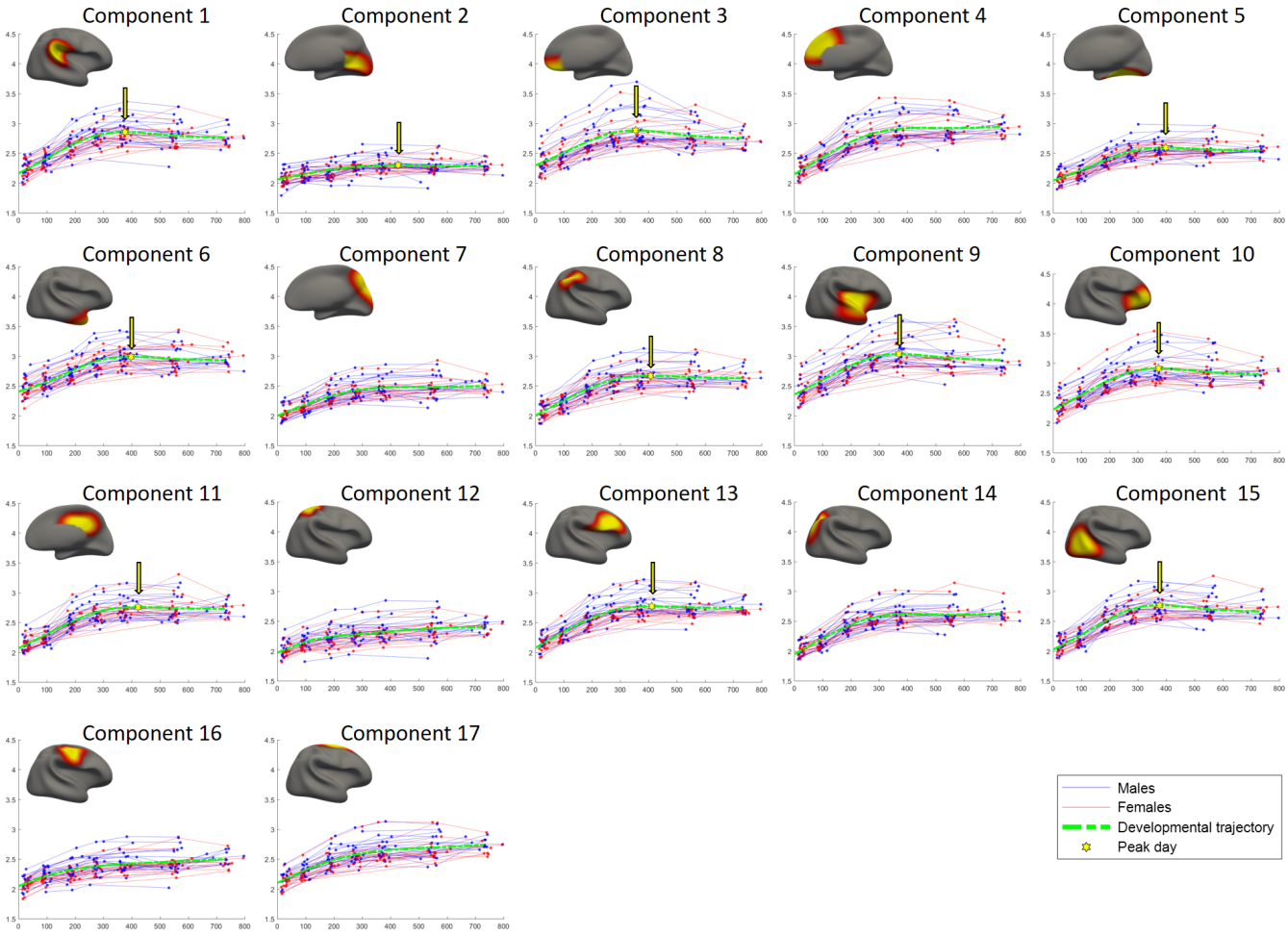

Fig. S4. Developmental trajectories of the average cortical thickness of each discovered region in the right hemisphere. The y-axis stands for CT and the x-axis represents the age in days. Red lines and blue lines represent females and males, respectively. The dashed green curve illustrates the fitted model of the population's trajectory of each region. The peak point of each fitted curve is signified using a yellow hexagon and an arrow (if exists).

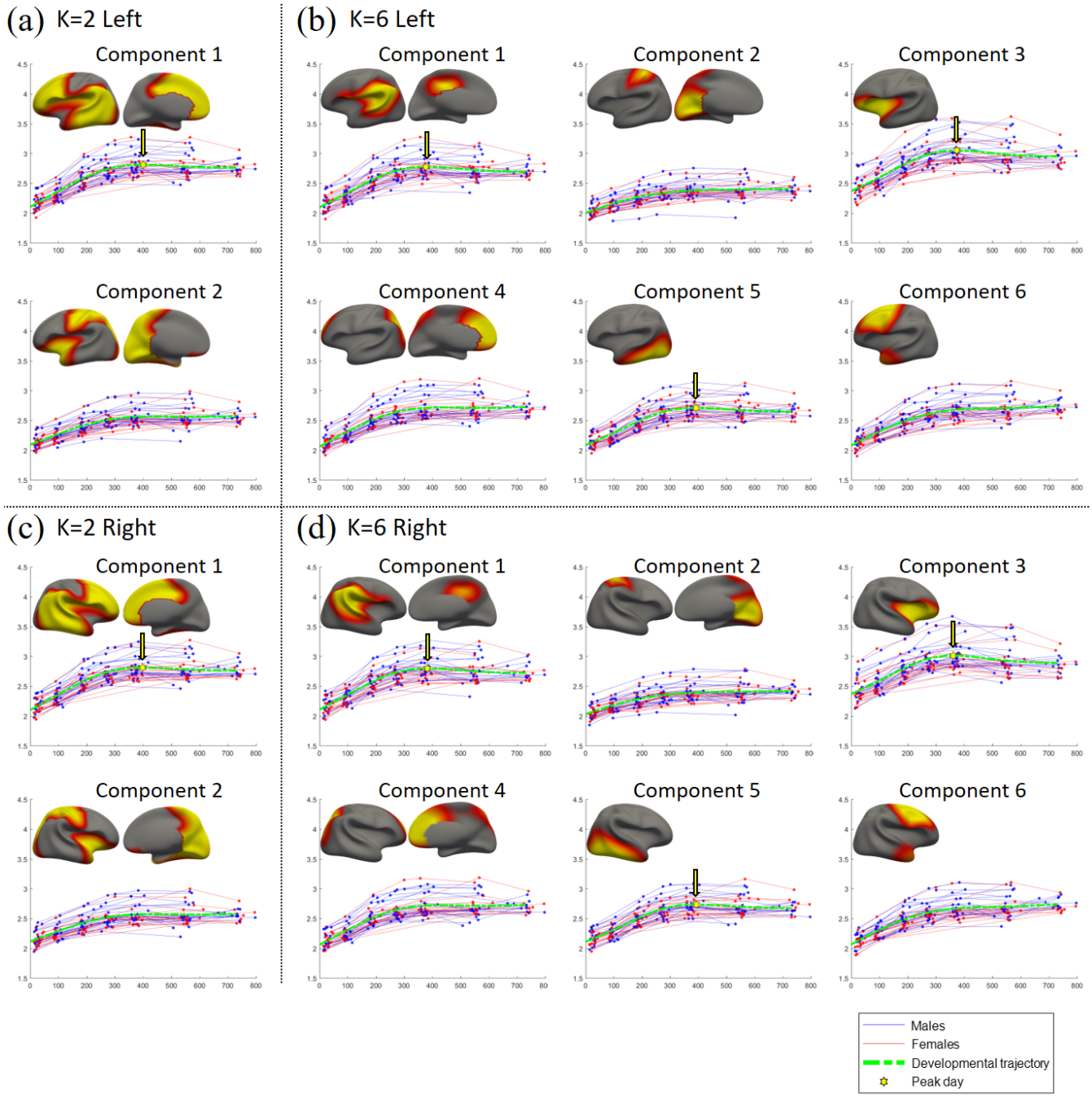

Fig. S5. Developmental trajectories of the average cortical thickness of each discovered region at K=2 in the (a) left and (c) right hemispheres, and K=6 in the (b) left and (d) right hemispheres. The y-axis stands for CT and the x-axis represents the age in days. Red lines and blue lines represent females and males, respectively. The dashed green curve illustrates the fitted model of the population's trajectory of each region. The peak point of each fitted curve is signified using a yellow hexagon and an arrow (if exists).

Table S1. Demographic information of each scanned age group of our longitudinal dataset.

Age group (Months)	Subject number	Gender (M/F)	Age range (Months)
1	33	19/14	0.47~1.60
3	31	19/12	2.73~3.87
6	32	19/13	5.73~7.50
9	30	18/12	8.73~10.13
12	31	17/14	11.73~13.93
18	33	17/16	16.90~20.43
24	20	7/13	22.20~26.57

Table S2. Comparison of the fitted generalized additive mixed models (GAMM, non-parametric), linear, quadratic and sigmoid (parametric) models in terms of the general cross validation (GCV) error. The significance of the fixed effect (*p*-value) is shown. The cortical thickness peak age (in days) with its 0.95 confidence interval estimated by the GAMM model is also shown (if exists).

	GAMM			Quadratic		Sigmoid		Linear		Sex difference
	GCV	Model p-value	Peak age	GCV	Model *p*-value	GCV	Model *p*-value	GCV	Model *p*-value	*p*-value
Left hemisphere	0.004158	8.01E-95	428±7.41	0.006543	3.11E-88	0.005424	5.42E-92	0.020241	1.49E-41	0.9080
Right hemisphere	0.004068	2.29E-95	426±7.7	0.006462	4.50E-88	0.005349	5.05E-92	0.020125	2.00E-41	0.7615
	K=2 regions									
Left-1	0.005108	1.87E-97	402±3.51	0.008687	6.27E-90	0.007071	2.81E-94	0.028658	1.36E-40	0.9087
Left-2	0.003586	6.13E-86	-	0.004925	5.43E-82	0.004302	2.18E-84	0.012845	2.92E-42	0.9012
Right-1	0.005013	3.00E-98	403±3.34	0.008580	8.17E-91	0.007059	8.62E-95	0.028897	8.40E-41	0.8132
Right-2	0.003652	8.65E-84	-	0.005012	4.17E-79	0.004317	2.22E-82	0.012622	3.11E-41	0.6956
	K=6 regions									
Left-1	0.005369	2.53E-93	371±1.82	0.009511	3.93E-83	0.006666	1.48E-89	0.029263	1.12E-36	0.9060
Left-2	0.003303	4.28E-75	-	0.003989	5.08E-74	0.003410	7.67E-76	0.008447	1.04E-42	0.8449
Left-3	0.007089	1.86E-86	368±1.63	0.011234	1.58E-76	0.009472	5.00E-79	0.034211	1.59E-32	0.8890
Left-4	0.005580	1.40E-90	-	0.008175	1.35E-86	0.005653	2.06E-90	0.023517	5.07E-43	0.9244
Left-5	0.004255	1.78E-96	387±2.14	0.007146	3.55E-88	0.005464	3.96E-88	0.024104	3.50E-39	0.8707
Left-6	0.006002	1.64E-84	-	0.007717	1.33E-85	0.005916	2.16E-83	0.018078	7.27E-49	0.7922
Right-1	0.006026	2.93E-90	378±1.88	0.010015	2.32E-82	0.007557	2.80E-87	0.030862	9.93E-36	0.6724
Right-2	0.003609	9.67E-71	-	0.004284	4.00E-70	0.003568	2.74E-71	0.008160	4.61E-42	0.5139
Right-3	0.008622	4.41E-76	355±1.63	0.012653	2.89E-66	0.011350	7.44E-70	0.035423	1.57E-27	0.8331
Right-4	0.005122	9.72E-94	-	0.007761	2.58E-89	0.005493	3.45E-92	0.023799	1.59E-43	0.7835
Right-5	0.003702	7.33E-101	391±2.24	0.006448	1.30E-91	0.004867	3.05E-90	0.023080	2.81E-41	0.7261
Right-6	0.005652	9.82E-87	-	0.007568	2.68E-86	0.006548	2.77E-85	0.017822	2.04E-49	0.7186
	k=17 regions									
Left-1	0.006083	8.30E-91	359±2.69	0.011097	1.12E-78	0.008730	9.56E-85	0.033376	1.97E-33	0.8384
Left-2	0.004223	1.36E-47	457±5.03	0.004587	3.05E-48	0.004198	3.98E-50	0.008284	3.53E-24	0.7041
Left-3	0.010805	2.17E-70	374±3.44	0.013974	3.95E-65	0.012745	6.86E-68	0.038889	3.36E-26	0.7647
Left-4	0.008850	4.64E-88	-	0.012181	2.38E-86	0.011023	6.73E-88	0.033531	1.33E-44	0.8495
Left-5	0.004122	4.19E-91	392±4.35	0.006383	1.86E-86	0.005819	3.96E-87	0.020826	5.61E-39	0.6229
Left-6	0.005911	1.89E-88	401±4.45	0.008542	9.53E-82	0.009180	2.36E-77	0.025289	4.76E-39	0.6136
Left-7	0.004738	4.45E-77	-	0.006027	5.68E-75	0.005195	2.50E-78	0.013580	6.03E-41	0.9170
Left-8	0.006144	2.93E-87	420±8.58	0.009323	1.66E-82	0.007283	8.89E-89	0.025949	1.20E-39	0.9665
Left-9	0.007439	2.81E-81	360±2.89	0.011476	2.67E-70	0.010217	9.40E-74	0.030997	2.85E-32	0.8689
Left-10	0.006737	2.69E-91	383±3.46	0.010811	7.94E-83	0.009147	4.09E-86	0.034671	1.40E-35	0.9392
Left-11	0.006095	1.63E-90	406±6.34	0.009293	6.48E-86	0.008155	1.19E-88	0.028529	1.50E-40	0.9331
Left-12	0.004576	3.08E-66	-	0.005026	6.26E-66	0.005939	1.47E-60	0.007224	5.14E-50	0.8956
Left-13	0.006496	1.30E-87	447±10.65	0.009523	1.82E-84	0.008151	2.40E-87	0.025937	1.02E-41	0.8935
Left-14	0.006730	2.70E-80	-	0.009407	1.43E-79	0.007587	1.89E-85	0.023043	1.14E-41	0.9777
Left-15	0.006324	2.75E-88	373±3.62	0.010384	4.22E-81	0.008701	1.02E-84	0.030342	4.84E-37	0.5817
Left-16	0.005751	9.39E-63	-	0.006193	2.47E-63	0.006953	1.66E-59	0.008807	6.19E-47	0.7568
Left-17	0.007285	2.23E-77	-	0.008256	7.12E-80	0.009762	2.94E-73	0.016142	4.96E-51	0.6254
Right-1	0.007744	6.82E-82	370±3.18	0.012089	1.59E-75	0.009864	5.94E-80	0.034595	1.30E-31	0.8072
Right-2	0.004318	2.97E-41	445±7.65	0.004700	9.59E-42	0.004328	2.70E-43	0.007035	3.42E-24	0.2655
Right-3	0.009475	1.56E-66	350±2.6	0.013034	2.68E-58	0.012115	6.49E-61	0.033255	4.02E-23	0.9427
Right-4	0.008189	1.61E-88	-	0.011310	8.81E-88	0.010773	1.65E-87	0.031570	5.33E-45	0.9130
Right-5	0.003348	9.05E-97	397±5.25	0.005317	1.03E-89	0.005357	2.76E-87	0.018010	6.65E-42	0.4315
Right-6	0.007172	5.66E-79	414±7.27	0.009413	2.37E-75	0.010486	9.77E-71	0.023703	7.39E-40	0.8044
Right-7	0.004427	1.84E-80	-	0.005631	1.58E-78	0.005049	4.87E-81	0.013431	2.16E-43	0.6332
Right-8	0.006783	4.15E-85	418±6.42	0.009949	8.44E-81	0.008193	4.01E-85	0.026695	1.16E-39	0.5287
Right-9	0.009080	4.45E-78	368±3.29	0.012762	1.66E-70	0.011504	1.20E-73	0.037106	1.07E-29	0.8991
Right-10	0.006890	6.14E-88	366±3.31	0.011145	1.63E-76	0.009109	9.28E-83	0.033289	4.57E-34	0.8343
Right-11	0.007257	9.10E-85	439±7.73	0.009901	1.49E-85	0.009792	2.34E-83	0.027646	5.10E-42	0.7803
Right-12	0.005066	4.85E-61	-	0.005484	2.25E-60	0.006268	2.59E-56	0.007347	1.14E-46	0.6622
Right-13	0.005840	8.79E-92	441±10.32	0.009198	1.06E-86	0.007224	2.37E-92	0.026964	3.30E-41	0.8499
Right-14	0.005978	4.05E-88	-	0.009121	3.15E-84	0.007255	1.95E-90	0.026056	5.05E-42	0.5543
Right-15	0.005279	5.48E-99	368±3.04	0.010127	6.31E-87	0.008520	1.64E-90	0.034961	3.53E-37	0.5717
Right-16	0.006181	2.82E-59	-	0.006763	1.25E-58	0.007025	1.23E-57	0.009222	8.41E-44	0.6973
Right-17	0.006814	4.14E-78	-	0.007668	1.49E-80	0.009297	2.80E-73	0.014460	9.23E-53	0.6444

Table S3. Significance of CT decrease from 18 to 24 months and 14 to 18 and 24 months for the whole brain, as well as the 17-regions in the left and right hemispheres (when peak age exists). Significant differences with $p < 0.05$ are marked in bold.

	Left hemisphere			Right hemisphere		
	18M-24M	14M-18M	14M-24M	18M-24M	14M-18M	14M-24M
Whole brain	3.58E-01	2.32E-01	5.99E-02	6.26E-01	2.79E-01	**4.35E-02**
Region 1	8.12E-01	1.08E-01	**2.78E-03**	8.62E-01	**3.09E-02**	**4.90E-03**
Region 2	7.63E-01	1.24E-01	3.37E-01	9.52E-01	9.70E-01	7.05E-02
Region 3	7.63E-01	**1.42E-03**	**2.85E-03**	7.22E-01	**1.72E-02**	**2.85E-03**
Region 4	-	-	-	-	-	-
Region 5	9.52E-01	2.67E-01	7.05E-02	8.38E-01	8.43E-01	7.05E-02
Region 6	8.38E-01	3.81E-01	**2.24E-02**	8.38E-01	8.78E-01	7.05E-02
Region 7	-	-	-	-	-	-
Region 8	7.22E-01	2.27E-01	7.05E-02	8.38E-01	3.73E-01	7.05E-02
Region 9	8.38E-01	**4.78E-02**	**4.42E-03**	8.38E-01	**1.66E-03**	**1.02E-02**
Region 10	8.38E-01	1.66E-01	**1.15E-02**	9.38E-01	2.27E-01	**1.62E-02**
Region 11	7.22E-01	5.88E-01	7.05E-02	8.38E-01	8.39E-01	7.05E-02
Region 12	-	-	-	-	-	-
Region 13	7.22E-01	1.95E-01	7.05E-02	7.22E-01	2.00E-01	8.47E-02
Region 14	-	-	-	-	-	-
Region 15	7.22E-01	7.41E-01	**1.62E-02**	9.52E-01	1.11E-01	**2.85E-03**
Region 16	-	-	-	-	-	-
Region 17	-	-	-	-	-	-

Table S4. Comparison of the peak ages (in days) estimated using all data and those only using small-sample data. Note that the small-sample data only include scans from subjects without any missing scan(s) at 12, 18 and 24 months. Significant differences are marked in bold with $p < 0.05$.

	Left hemisphere			Right hemisphere		
	All data	Small data	Significance	All data	Small data	Significance
Whole brain	428±7.41	417±9.87	5.60E-01	426±7.7	418±11.93	8.67E-01
Region 1	359±2.68	361±3.37	6.86E-01	370±3.16	370±3.27	1.21E+00
Region 2	457±4.94	440±7.9	**2.53E-03**	445±6.66	462±6.62	3.91E-01
Region 3	374±3.42	370.±3.16	2.00E-01	350±2.58	367±3.18	**5.34E-03**
Region 4	-	-	-	-	-	-
Region 5	392±4.16	407±5.15	**1.24E-04**	397±3.86	415±5.31	**1.95E-05**
Region 6	401±4.21	394±2.63	**2.29E-02**	414±4.91	404±3.94	3.64E-01
Region 7	-	-	-	-	-	-
Region 8	420±5.26	392±5.2	**9.54E-09**	418±4.63	423±3.12	3.20E-01
Region 9	360±2.87	360±3.13	1.13E+00	368±3.27	373±4.13	2.22E-01
Region 10	383±3.43	369±3.22	**1.00E-07**	366±3.26	379±3.79	**1.22E-05**
Region 11	406±4	412±4.11	2.00E-01	439±4.71	458±5.17	1.31E-01
Region 12	-	-	-	-	-	-
Region 13	447±5.83	440±3.6	2.00E-01	441±5.16	439±3.96	1.04E+00
Region 14	-	-	-	-	-	-
Region 15	373±3.46	375±4.02	7.99E-01	368±2.99	378±3.52	3.91E-01
Region 16	-	-	-	-	-	-
Region 17	-	-	-	-	-	-

Table S5. Significance testing between scans with and without follow-up scans at 24 months. Specifically, we grouped scans at each time point based on their existence of 24 months follow-up scans. The Wilcoxon test was performed to test significant differences of CT between these two groups. No significant effect was found at the significance level of $p < 0.05$.

	Birth	3M	6M	9M	12M	18M
Left hemisphere	6.75E-02	1.46E-01	3.38E-01	1.59E-01	2.10E-01	7.03E-01
Right hemisphere	6.75E-02	1.46E-01	3.71E-01	1.59E-01	2.11E-01	7.03E-01
Left-1	6.75E-02	1.37E-01	3.71E-01	1.60E-01	2.10E-01	7.03E-01
Left-2	3.96E-01	7.05E-01	6.91E-01	1.60E-01	3.43E-01	7.30E-01
Left-3	1.28E-01	4.28E-01	3.71E-01	1.59E-01	2.11E-01	7.03E-01
Left-4	6.75E-02	1.37E-01	3.22E-01	1.59E-01	2.10E-01	7.03E-01
Left-5	1.52E-01	1.54E-01	3.22E-01	1.59E-01	2.10E-01	7.03E-01
Left-6	6.75E-02	1.37E-01	3.22E-01	1.67E-01	2.10E-01	7.03E-01
Left-7	8.21E-02	1.37E-01	3.30E-01	3.41E-01	2.20E-01	7.03E-01
Left-8	6.75E-02	2.04E-01	5.34E-01	3.13E-01	2.54E-01	7.15E-01
Left-9	6.75E-02	1.37E-01	3.59E-01	2.24E-01	2.77E-01	7.03E-01
Left-10	6.75E-02	1.46E-01	3.22E-01	2.24E-01	2.10E-01	7.03E-01
Left-11	7.32E-02	1.37E-01	3.22E-01	1.59E-01	2.10E-01	7.03E-01
Left-12	7.32E-02	8.13E-01	9.13E-01	4.10E-01	6.64E-01	8.45E-01
Left-13	6.75E-02	1.46E-01	3.22E-01	1.60E-01	2.22E-01	7.53E-01
Left-14	1.59E-01	1.37E-01	3.22E-01	2.54E-01	3.76E-01	7.53E-01
Left-15	7.32E-02	1.37E-01	3.22E-01	1.63E-01	2.11E-01	7.03E-01
Left-16	7.32E-02	2.82E-01	3.72E-01	1.59E-01	2.10E-01	7.53E-01
Left-17	7.32E-02	1.46E-01	3.71E-01	1.67E-01	2.22E-01	7.53E-01
Right-1	6.75E-02	1.37E-01	4.13E-01	1.63E-01	2.10E-01	7.43E-01
Right-2	7.32E-02	9.84E-01	9.55E-01	4.26E-01	4.78E-01	7.50E-01
Right-3	9.71E-02	1.46E-01	5.91E-01	1.59E-01	3.62E-01	7.50E-01
Right-4	6.75E-02	1.37E-01	3.22E-01	1.59E-01	2.49E-01	7.03E-01
Right-5	7.32E-02	1.46E-01	3.22E-01	1.60E-01	2.10E-01	7.03E-01
Right-6	7.12E-02	1.37E-01	3.47E-01	1.59E-01	2.10E-01	7.03E-01
Right-7	9.71E-02	3.20E-01	6.06E-01	4.93E-01	6.03E-01	8.45E-01
Right-8	7.32E-02	3.07E-01	5.05E-01	1.92E-01	3.62E-01	8.45E-01
Right-9	6.75E-02	1.37E-01	3.72E-01	1.59E-01	2.10E-01	7.03E-01
Right-10	6.75E-02	1.37E-01	3.22E-01	1.59E-01	2.10E-01	7.03E-01
Right-11	6.75E-02	1.37E-01	3.22E-01	1.67E-01	2.10E-01	7.03E-01
Right-12	2.92E-01	4.28E-01	6.77E-01	4.10E-01	6.33E-01	8.45E-01
Right-13	6.75E-02	2.95E-01	3.22E-01	1.59E-01	2.25E-01	7.53E-01
Right-14	9.40E-02	1.46E-01	4.51E-01	3.41E-01	5.46E-01	9.27E-01
Right-15	6.75E-02	1.37E-01	3.22E-01	1.59E-01	2.10E-01	7.03E-01
Right-16	6.75E-02	1.37E-01	3.87E-01	1.60E-01	2.25E-01	7.50E-01
Right-17	1.52E-01	1.37E-01	3.87E-01	3.13E-01	2.65E-01	8.45E-01

Table S6. Global CT measurements from birth to 24 months of age for both vertex-wise and region-wise averages of CT values, calculated for the whole brain, the left hemisphere, and the right hemisphere, respectively.

	Vertex-wise average (mm)			Region-wise average (mm)		
	Both hemispheres	Left hemisphere	Right hemisphere	Both hemispheres	Left hemisphere	Right hemisphere
Birth	2.1025	2.0984	2.1066	2.1110	2.1070	2.1150
1M	2.1683	2.1645	2.1720	2.1755	2.1721	2.1789
2M	2.2359	2.2325	2.2393	2.2420	2.2392	2.2449
3M	2.3028	2.2997	2.3059	2.3079	2.3055	2.3103
4M	2.3682	2.3653	2.3711	2.3727	2.3707	2.3748
5M	2.4313	2.4285	2.4341	2.4355	2.4337	2.4373
6M	2.4905	2.4877	2.4933	2.4946	2.4930	2.4963
7M	2.5444	2.5415	2.5472	2.5486	2.5470	2.5501
8M	2.5913	2.5884	2.5941	2.5958	2.5943	2.5973
9M	2.6299	2.6270	2.6327	2.6345	2.6331	2.6360
10M	2.6588	2.6560	2.6616	2.6636	2.6622	2.6649
11M	2.6786	2.6759	2.6812	2.6834	2.6821	2.6846
12M	2.6907	2.6882	2.6932	2.6954	2.6943	2.6965
13M	2.6966	2.6943	2.6988	2.7011	2.7002	2.7020
14M	2.6976	2.6955	2.6996	2.7019	2.7011	2.7027
15M	2.6952	2.6933	2.6970	2.6993	2.6986	2.6999
16M	2.6908	2.6891	2.6924	2.6946	2.6941	2.6951
17M	2.6858	2.6842	2.6873	2.6893	2.6888	2.6897
18M	2.6807	2.6793	2.6820	2.6841	2.6837	2.6844
19M	2.6765	2.6752	2.6777	2.6801	2.6798	2.6804
20M	2.6731	2.6719	2.6742	2.6773	2.6770	2.6776
21M	2.6704	2.6693	2.6714	2.6755	2.6753	2.6758
22M	2.6682	2.6672	2.6691	2.6744	2.6742	2.6747
23M	2.6660	2.6651	2.6669	2.6738	2.6736	2.6741
24M	2.6638	2.6630	2.6646	2.6735	2.6733	2.6736

References

1. Lyall AE, et al. (2014) Dynamic development of regional cortical thickness and surface area in early childhood. *Cerebral cortex* 25(8):2204–2212.
2. Blumenthal JD, Zijdenbos A, Molloy E, Giedd JN (2002) Motion artifact in magnetic resonance imaging: implications for automated analysis. *Neuroimage* 16(1):89–92.
3. Li G, et al. (2015) Construction of 4d high-definition cortical surface atlases of infants: Methods and applications. *Medical image analysis* 25(1):22–36.
4. Li G, Lin W, Gilmore JH, Shen D (2015) Spatial patterns, longitudinal development, and hemispheric asymmetries of cortical thickness in infants from birth to 2 years of age. *Journal of Neuroscience* 35(24):9150–9162.
5. Li G, et al. (2012) Mapping region-specific longitudinal cortical surface expansion from birth to 2 years of age. *Cerebral cortex* 23(11):2724–2733.
6. Geng X, et al. (2017) Structural and maturational covariance in early childhood brain development. *Cerebral Cortex* 27(3):1795–1807.
7. Meng Y, et al. (2018) Discovering cortical sulcal folding patterns in neonates using large-scale dataset. *Human Brain Mapping*.
8. Li G, et al. (2014) Mapping longitudinal development of local cortical gyrification in infants from birth to 2 years of age. *Journal of Neuroscience* 34(12):4228–4238.
9. Jha SC, et al. (2018) Environmental influences on infant cortical thickness and surface area. *Cerebral Cortex*.
10. Meng Y, Li G, Gao Y, Lin W, Shen D (2016) Learning-based subject-specific estimation of dynamic maps of cortical morphology at missing time points in longitudinal infant studies. *Human brain mapping* 37(11):4129–4147.
11. Smith SM, et al. (2004) Advances in functional and structural mr image analysis and implementation as fsl. *Neuroimage* 23:S208–S219.
12. Shi F, et al. (2012) Label: pediatric brain extraction using learning-based meta-algorithm. *Neuroimage* 62(3):1975–1986.
13. Shen D, Davatzikos C (2002) Hammer: hierarchical attribute matching mechanism for elastic registration. *IEEE transactions on medical imaging* 21(11):1421–1439.
14. Sled JG, Zijdenbos AP, Evans AC (1998) A nonparametric method for automatic correction of intensity nonuniformity in mri data. *IEEE transactions on medical imaging* 17(1):87–97.
15. Wang L, Shi F, Lin W, Gilmore JH, Shen D (2011) Automatic segmentation of neonatal images using convex optimization and coupled level sets. *NeuroImage* 58(3):805–817.
16. Wang L, et al. (2014) Integration of sparse multi-modality representation and anatomical constraint for isointense infant brain mr image segmentation. *NeuroImage* 89:152–164.
17. Wang L, et al. (2012) 4d multi-modality tissue segmentation of serial infant images. *PLOS ONE* 7(9).
18. Wang L, et al. (2015) Links: Learning-based multi-source integration framework for segmentation of infant brain images. *NeuroImage* 108:160–172.
19. Li G, et al. (2014) Measuring the dynamic longitudinal cortex development in infants by reconstruction of temporally consistent cortical surfaces. *NeuroImage* 90:266–279.
20. Li G, Nie J, Shen D (2011) Consistent reconstruction of cortical surfaces from longitudinal brain mr images in *MICCAI'11 Proceedings of the 14th international conference on Medical image computing and computer-assisted intervention - Volume Part II*. Vol. 14, pp. 671–679.
21. Fischl B, Sereno MI, Dale AM (1999) Cortical surface-based analysis ii: Inflation, flattening, and a surface-based coordinate system. *NeuroImage* 9(2):195–207.
22. Lee DD, Seung HS (1999) Learning the parts of objects by non-negative matrix factorization. *Nature* 401(6755):788–791.
23. Yang Z, Oja E (2010) Linear and nonlinear projective nonnegative matrix factorization. *IEEE Transactions on Neural Networks* 21(5):734–749.
24. Wu S, et al. (2016) Stability-driven nonnegative matrix factorization to interpret spatial gene expression and build local gene networks. *Proceedings of the National Academy of Sciences of the United States of America* 113(16):4290–4295.
25. Rousseeuw PJ (1987) Silhouettes: a graphical aid to the interpretation and validation of cluster analysis. *Journal of Computational and Applied Mathematics* 20(1):53–65.
26. Chen CH, et al. (2013) Genetic topography of brain morphology. *Proceedings of the National Academy of Sciences of the United States of America* 110(42):17089–17094.
27. Lin X, Zhang D (1999) Inference in generalized additive mixed modelsby using smoothing splines. *Journal of the royal statistical society: Series b (statistical methodology)* 61(2):381–400.
28. Eubank RL, Spiegelman CH (1990) Testing the goodness of fit of a linear model via nonparametric regression techniques. *Journal of the American Statistical Association* 85(410):387–392.
29. Staniswalis JG, Severini TA (1991) Diagnostics for assessing regression models. *Journal of the American Statistical Association* 86(415):684–692.
30. Ye J (1998) On measuring and correcting the effects of data mining and model selection. *Journal of the American Statistical Association* 93(441):120–131.
31. Sherman M, Cessie Sl (1997) A comparison between bootstrap methods and generalized estimating equations for correlated outcomes in generalized linear models. *Communications in Statistics-Simulation and Computation* 26(3):901–925.